


# Quantitative estimation of coercive field in a ferromagnetic grain using field sweep simulation

Masamichi Nishino <sup>1,2,3,\*</sup> and Seiji Miyashita<sup>4,5,3</sup>

<sup>1</sup>Research Center for Advanced Measurement and Characterization, National Institute for Materials Science, 1-2-1 Sengen, Tsukuba, Ibaraki 305-0047, Japan

<sup>2</sup>Research Center for Materials Nanoarchitectonics, National Institute for Materials Science, 1-1 Namiki, Tsukuba, Ibaraki 305-0044, Japan

<sup>3</sup>Elements Strategy Initiative Center for Magnetic Materials, National Institute for Materials Science, 1-2-1 Sengen, Tsukuba, Ibaraki 305-0047, Japan

<sup>4</sup>Department of Physics, Graduate School of Science, The University of Tokyo, 7-3-1 Hongo, Tokyo 113-0033, Japan

<sup>5</sup>Physical Society of Japan, 2-31-22 Yushima, Tokyo 113-0033, Japan



(Received 18 August 2022; revised 28 March 2023; accepted 1 May 2023; published 10 May 2023)

High coercivity is an important property of permanent magnets for application in energy conversion devices. The Nd magnet,  $\text{Nd}_2\text{Fe}_{14}\text{B}$ , is a typical material. Because coercivity is a long-time relaxation phenomenon, which originates from a strong metastable magnetic state, it is difficult to estimate coercive field (coercive force) studying the time evolution dynamics simulation of a model with atomistic parameters under the limitation of the simulation time. In our recent study [M. Nishino *et al.*, *Phys. Rev. B* **102**, 020413(R) (2020)], we presented a method to estimate coercivity using a statistical method to extend the limitation of simulation time and evaluated appropriately the coercive field of a single grain of the Nd magnet. In the present study, we propose an alternative method to estimate coercivity more conveniently using the field-dependent survival (nonreversal) probability generated by a time evolution simulation under a field sweep. We demonstrate that the coercive field of the single grain can be estimated. In this method, not only coercive field but also the zero-field energy barrier and field for the zero-energy barrier can be estimated. We discuss detailed features of the estimation of these quantities.

DOI: [10.1103/PhysRevB.107.184422](https://doi.org/10.1103/PhysRevB.107.184422)

## I. INTRODUCTION

Realization of high efficiency in energy conversion devices is a crucial issue for safe energy technology toward sustainable development goals. High-coercivity permanent magnets such as the neodymium (Nd) magnet,  $\text{Nd}_2\text{Fe}_{14}\text{B}$  [1–9], play an important role. The Nd magnet is used in various electronic devices, e.g., motors, generators, and compressors, and efforts to increase the coercivity have been performed [10–13]. Coercive field  $H_c$  is caused by a hysteresis nature of magnets, i.e., a nonequilibrium dynamical phenomenon. It depends not only on the property of the hard magnet phase but also on those of grain boundary, grain shape, etc. [14–22]. Therefore, the coercivity mechanism is still a difficult issue to be solved.

At finite temperatures, the Stoner-Wohlfarth mechanism, i.e., coherent rotation, does not hold in the magnetization reversal process, but the nucleation process is important because it is the trigger of magnetization reversal [23–25]. Nucleation occurs in a small region, i.e., nm scale, and to understand the microscopic process of nucleation, recently developed atomistic models [19,26–41] are quite useful.

Unlike continuum modelings developed in micromagnetism [42], in atomistic modelings, the lattice structure (Fig. 1) is introduced with atomic-scale magnetic parameters, estimated from first-principles computation or from experi-

mental analyses. Therefore, magnetic properties reflect the details of the microscopic structure. Furthermore, atomistic modelings have another merit. The temperature effect can be analyzed properly treating all atom spins with the stochastic Landau-Lifshitz-Gilbert (SLLG) equation [43,44] or Monte Carlo (MC) methods, which generate canonical distribution in the equilibrium at a given temperature. Using the atomistic models, finite-temperature properties of the Nd magnet have recently been investigated. Quantitative analyses on the temperature dependence of magnetization accompanying a spin-reorientation transition [26–28,36,39], domain wall profiles [27,30,37,38], surface effects to magnetization reversal [30,40], nucleation features [19,32,33], ferromagnetic resonance [31], dysprosium substitution effect [41], etc., have been intensively performed.

The estimation of coercive field from microscopic information of magnets is an important subject and various attempts have been made. It should be noted that the bulk magnet consists of many grains and grain boundaries, and the estimation of the coercive field of the bulk is difficult (practically impossible) using atomistic models at the present state because of large degrees of freedom. To study fundamental information of the coercivity, the coercive field of a single grain has been estimated based on an atomistic model [32,33].

Coercive field has been studied from the viewpoint of a free-energy barrier. The minimum energy path method has been used to obtain the change of the free energy along a path of evolution of magnetization from a metastable to stable state

\*Corresponding author: [nishino.masamichi@nims.go.jp](mailto:nishino.masamichi@nims.go.jp)

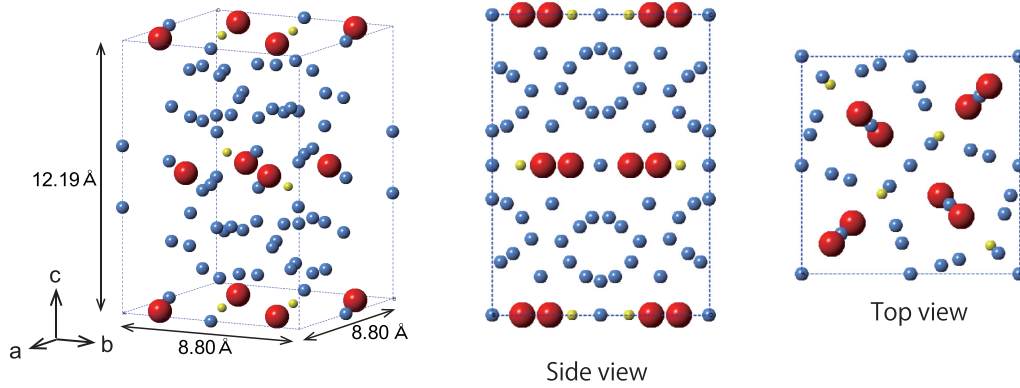


FIG. 1. Unit cell of  $\text{Nd}_2\text{Fe}_{14}\text{B}$ . Blue, red, and yellow balls denote Fe, Nd, and B atoms, respectively.

[45,46]. For atomistic model studies, the angular dependence of the free energy of the hard magnet phase of the Nd magnet was estimated [26] using the constrained Monte Carlo method [47]. The free energy of a single grain of the Nd magnet as a function of the field was obtained from the concept of thermal activation [33].

Coercivity is a phenomenon of a nonequilibrium long-time relaxation process, and to approach the mechanism of coercivity, time evolution dynamics analyses are important. However, there exists a difficulty in time evolution dynamics simulations, i.e., simulation time. Experimentally coercive field is defined as a field at which the relaxation time is 1 s. On the other hand, a practical simulation time is around 1 ns, and it is too short to study such a long-time relaxation process. Simulation time is a common problem to studies on long-time relaxation phenomena in all real systems, e.g., biological systems.

Recently, we proposed a method to estimate the coercive field to extend the limitation of simulation time in Ref. [32]. In this method, first, we performed a simulation of magnetization reversal for many samples in a fixed time period ( $t < 1$  ns) under a fixed field, and observed the survival (unrelaxed) probability as a function of time ( $t$ ). Then, using a statistical relation to the probability, we determined the relaxation time. There the relaxation time could be estimated up to microseconds or submicroseconds. Finally, we estimated the field for the 1 s relaxation time by an extrapolation of the relaxation time. Using this method, we estimated the coercive field of a single grain to be  $H_c \simeq 3.0\text{--}3.2$  T. This was consistent with the value estimated for the same grain by a MC study [33] with the Wang-Landau algorithm [48]. In this MC study, the field dependence of the free-energy barrier was compared to  $\Delta F$  corresponding to 1 s Arrhenius relaxation time,  $\tau = \tau_0 \exp(\beta \Delta F)$ , where  $\tau_0$  is a prefactor and  $\beta$  is the inverse temperature.

The above-mentioned two methods require very heavy computational costs with complexity. For the study of coercivity in various situations, we need a more convenient method to obtain the coercivity. In the present study we show an alternative convenient method to estimate coercivity. We demonstrate that the coercive field of the same single grain can be estimated with high accuracy using a field sweep (less than 1 ns).

There are three kinds of the (free) energy shape for magnetization reversal as shown in Fig. 2, i.e., barrier crossing type, marginal type, and no-barrier type, which lead to stochastic, intermediate, and deterministic dynamics, respectively. In contrast to the experiments, only a short-time measurement is allowed in a time evolution dynamics simulation. Therefore, in the present paper, we consider the survival (nonreversal) probability extending the field sweep range from the stochastic region to the deterministic region whose relaxation time is much shorter than the stochastic one. We show that the coercive field is estimated with high accuracy and also present the estimation of the zero-field energy barrier and field for the zero-energy barrier, which are important for the analysis of the metastable property.

The rest of the paper is organized as follows. In Sec. II, the atomistic model for the Nd magnet is explained. In Sec. III, the time evolution dynamics method to estimate the coercivity is presented. In Sec. IV, the results and discussion are given. Section V is devoted to the summary.

## II. MODEL

We adopt the following atomistic Hamiltonian for the Nd magnet:

$$\mathcal{H} = - \sum_{i < j} 2J_{ij} \mathbf{s}_i \cdot \mathbf{s}_j - \sum_i^{Fe} D_i (s_i^z)^2 + \sum_i^{Nd} \sum_{l,m} \Theta_{l,i} A_{l,i}^m \langle r^l \rangle_i \hat{O}_{l,i}^m - H \sum_i S_i^z. \quad (1)$$

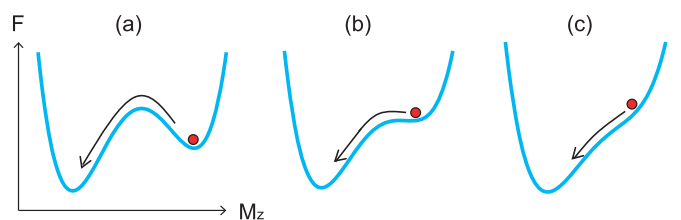


FIG. 2. Typical energy barrier types for magnetization reversal. (a) Barrier crossing type, (b) marginal type, and (c) no-barrier type, which lead to stochastic, intermediate, and deterministic dynamics, respectively.

Here,  $J_{ij}$  is the exchange interaction between the  $i$ th and  $j$ th sites, and  $D_i$  is the magnetic anisotropy constant for Fe atoms. The third term is the crystal electric field energy of Nd atoms, and  $\Theta_{l,i}$ ,  $A_{l,i}^m$ ,  $\langle r^l \rangle_i$ , and  $\hat{O}_{l,i}^m$  are the Stevens factor, coefficient of the spherical harmonics of the crystalline electric field, average of  $r^l$  over the radial wave function, and Stevens operator, respectively. We consider  $l = 2, 4, 6$  and  $m = 0$  (diagonal operators), which provide the dominant contribution. The fourth term is the Zeeman term, and  $H$  is the external magnetic field. For Fe and B atoms,  $s_i$  denote the magnetic moment at the  $i$ th site, while for Nd atoms, it is the moment of the valence ( $5d$  and  $6s$ ) electrons. The total moment for Nd atoms at the  $i$ th site is  $S_i = s_i + \mathcal{J}_i$ , where  $\mathcal{J}_i = g_T \mathbf{J}_i \mu_B$  with the magnitude of the total angular momentum,  $J = 9/2$ , and Landé  $g$  factor,  $g_T = 8/11$ . We define  $s_i = s_i$  for Fe and B atoms.

The details of the model are given in our previous papers [26–28,39], in which the magnetic interactions were mainly obtained from first-principles computation methods. We showed the spin-reorientation transition temperature,  $T_r = 150$  K, which is close to the experimentally estimated temperature [7–9,49], and the critical temperature,  $T_c \sim 870$  K, which is a little overestimated from the experimental values  $T_c \sim 600$  K [4,7], due to an overestimation of the exchange interactions. We are interested in room temperature properties and set  $T = 400$  K  $\simeq 0.46T_c$ , which is close to room temperature practically.

### III. DYNAMICAL METHOD

#### A. Real time dynamics with thermal fluctuation effect

We employ the SLLG equation [43,44] to study the time evolution dynamics of the Nd magnet:

$$\begin{aligned} \frac{d}{dt} \mathbf{S}_i = & -\frac{\gamma}{1 + \alpha_i^2} \mathbf{S}_i \times (\mathbf{H}_i^{\text{eff}} + \boldsymbol{\xi}_i) \\ & - \frac{\alpha_i \gamma}{(1 + \alpha_i^2) S_i} \mathbf{S}_i \times [\mathbf{S}_i \times (\mathbf{H}_i^{\text{eff}} + \boldsymbol{\xi}_i)]. \end{aligned} \quad (2)$$

Here  $\alpha_i$  is the Gilbert damping factor at the  $i$ th site and  $\gamma$  is the gyromagnetic constant.  $\mathbf{H}_i^{\text{eff}} = -\frac{\partial \mathcal{H}}{\partial \mathbf{S}_i}$  is the effective field applied at the  $i$ th site from the exchange interactions, anisotropy terms, and Zeeman term, and  $\boldsymbol{\xi}_i(t) = (\xi_i^x, \xi_i^y, \xi_i^z)$  is a white-Gaussian noise field with the following properties:

$$\langle \xi_i^\mu(t) \rangle = 0, \quad \langle \xi_i^\mu(t) \xi_j^\nu(s) \rangle = 2\mathcal{D}_i \delta_{ij} \delta_{\mu\nu} \delta(t - s). \quad (3)$$

The temperature of the system,  $T$ , is a function of the strength of the random noise field  $\mathcal{D}_i$  according to the fluctuation dissipation relation:

$$D_i = \frac{\alpha_i k_B T}{S_i \gamma}. \quad (4)$$

When this relation is satisfied, the system relaxes to the equilibrium state in the canonical distribution at temperature  $T$ . The value of  $\alpha_i$  is unknown for the Nd magnet, and we assume  $\alpha_i = \alpha = 0.1$ , which is a typical value for magnets [42].

We apply a kind of middle-point method [44] equivalent to the Heun method [43] for the numerical integration of the stochastic differential equation in the Stratonovich interpretation. For the time step of this equation,  $\Delta t = 0.1$  fs is used.

#### B. Survival probability under field sweep

For a weak reversed magnetic field, a magnetization reversal occurs in a barrier crossing process as shown in Fig. 2(a), which leads to a stochastic dynamics. The relaxation rate for the stochastic dynamics is given by the Arrhenius rate as

$$R = \frac{1}{\tau_0} e^{-\beta E_B(H)}, \quad (5)$$

where  $\tau_0$  is a preexponential factor, which represents of the frequency of the contact with the bath and is of order of the lattice vibration frequency. We adopt a commonly used value for the factor, i.e.,  $\tau_0 = 10^{-11}$  s [23], which was used in the paper giving the reference data [33].

On the other hand, for a strong reversed field, a magnetization reversal occurs deterministically as shown in Fig. 2(c). For the deterministic process, the relaxation rate is set to constant:

$$R = \text{const}. \quad (6)$$

The relaxation rate should vary with the field even in the deterministic region, but it is much faster than that in the stochastic region, and thus the choice is not relevant to estimate the coercive field.

For an intermediate field, the dynamics has a crossover feature [Fig. 2(b)]. In the present study, we consider an approximate form of relaxation rate which describes both the stochastic and deterministic regions including the crossover (intermediate) field region:

$$R = \frac{1}{\tau_0 (e^{\beta E_B(H)} + c)}, \quad (7)$$

which satisfies  $R \simeq \frac{1}{\tau_0} e^{-\beta E_B(H)}$  for positive large values of  $E_B(H)$  corresponding to the stochastic region, and  $R \simeq 1/(\tau_0 c)$  for small values of  $E_B(H)$  corresponding to the deterministic region. Using this probability  $R$ , we derive the probability of nonrelaxation when the field is swept until  $H$  starting from  $H = -\infty$  (all down state) as follows.

Since the relaxation rate at time  $t$  is  $R(H(t))$ , if a magnetization reversal does not occur until time  $t$ , the probability of avoiding magnetization reversal at  $t + \Delta t$  is given as  $1 - R(H(t))\Delta t = e^{-R(H(t))\Delta t} + O(\Delta t^2)$ . Then, the probability of avoiding magnetization reversal during the time  $[t_0, t]$ , where  $\Delta t = (t - t_0)/n$ , is described as

$$\begin{aligned} P(t) = & [1 - R(H(t_0))\Delta t][1 - R(H(t_0 + \Delta t))\Delta t] \\ & \times [1 - R(H(t_0 + 2\Delta t))\Delta t] \cdots [1 - R(H(t - \Delta t))\Delta t] \\ = & e^{-R(H(t_0))\Delta t} e^{-R(H(t_0 + \Delta t))\Delta t} \cdots e^{-R(H(t - \Delta t))\Delta t} + O(\Delta t) \\ = & \prod_{m=0}^{n-1} [e^{-R(H(t_0 + m\Delta t))\Delta t}] + O(\Delta t). \end{aligned} \quad (8)$$

For  $n \rightarrow \infty$  ( $\Delta t \rightarrow 0$ ) and  $t_0 \rightarrow -\infty$ , the probability is given as

$$P(t) = \exp \left[ -\frac{1}{\tau_0} \int_{-\infty}^t \frac{1}{e^{\beta E_B(H(t'))} + c} dt' \right]. \quad (9)$$

If the field is swept linearly with time, i.e.,  $H(t) = vt$ , then the probability as a function of  $H$  is given as

$$P(H) = \exp \left[ -\frac{1}{\tau_0} \int_{H(-\infty)=-\infty}^{H(t)} \frac{1}{e^{\beta E_B(h)} + c} \frac{dt}{dh} dh \right] \\ = \exp \left[ -\frac{1}{v\tau_0} \int_{-\infty}^H \frac{1}{e^{\beta E_B(h)} + c} dh \right]. \quad (10)$$

In the present work, we use the following formula for the (free) energy barrier:

$$E_B(H) = E_0 \left( 1 - \frac{H}{H_0} \right)^n, \quad (11)$$

where  $E_0$  is the zero-field energy barrier and  $H_0$  is the field for zero-energy barrier. This formula has often been employed for studies of magnetization reversal in permanent magnets [21,50,51].

The value of the exponent  $n$  is established as  $n = 1 \sim 2$  for many magnetic materials. For coherent magnetic reversal as in the Stoner-Wohlfarth model, the exponent is  $n = 2$  [52]. Givord *et al.* studied a thermally activated magnetization reversal using  $n = 1$  based on an experimental observation of field independence in the fluctuation field,  $S_v = k_B T / (\frac{\partial E_B}{\partial H})_T$ , for several Nd-Fe-B magnets [23,24].  $n = 1$  was also suggested for weak domain pinning [53], and then  $n = 1$  was experimentally observed as the domain wall pinning process in several magnets [54,55].

Recently,  $n \simeq 1$  for several Nd-Fe-B magnets was experimentally determined for a nucleation process [21,51] using a magnetic viscosity measurement and the Sharrock equation [56,57] (relation of coercivity vs reversal time).  $n \simeq 1$  was also confirmed by an experiment observing the reversal probability against a field sweep [51].  $n = 1$  was theoretically suggested in a recent nucleation model study [58] and in a Monte Carlo study for the Nd magnet atomistic model [33]. Therefore, in the present study, we adopt  $n = 1$  primarily. We also investigate the case of  $n = 2$  in the Appendix and discuss the difference between the two cases.

For  $E_B(H) = E_0(1 - \frac{H}{H_0})$ , i.e., the  $n = 1$  case,  $P(H)$  is given as

$$P(H) = \exp \left[ -\frac{1}{v\tau_0} \int_{-\infty}^H \frac{1}{e^{\beta E_0(1-\frac{h}{H_0})} + c} dh \right] \quad (12)$$

$$= \exp \left[ -\frac{1}{v\tau_0} e^{-\beta E_0} \int_{-\infty}^H \frac{1}{e^{-\frac{\beta E_0}{H_0} h} + c e^{-\beta E_0}} dh \right]. \quad (13)$$

Using the relation

$$\int \frac{dx}{\lambda + e^{\kappa x}} = \frac{1}{\lambda \kappa} (\kappa x - \ln |\lambda + e^{\kappa x}|) \quad (14)$$

with

$$\lambda = c e^{-\beta E_0}, \quad \kappa = -\frac{\beta E_0}{H_0}, \quad (15)$$

we have

$$P(H) = \exp \left[ -\frac{H_0}{c v \tau_0 \beta E_0} \ln \left( 1 + c e^{-\beta E_0(1-\frac{H}{H_0})} \right) \right]. \quad (16)$$

Then we have

$$\ln \{-\ln[P(H)]\} = \ln \left[ \frac{H_0}{c v \tau_0 \beta E_0} \ln \left( 1 + c e^{-\beta E_0(1-\frac{H}{H_0})} \right) \right]. \quad (17)$$

For  $c \rightarrow 0$ , i.e., the pure Arrhenius case,

$$\ln \{-\ln[P(H)]\} = \frac{\beta E_0}{H_0} H + \ln \left[ \frac{H_0}{v \tau_0 \beta E_0} \right], \quad (18)$$

which is a linear function of the field  $H$ . Therefore, a linear dependence of  $H$  for  $\ln \{-\ln[P(H)]\}$  indicates that a stochastic dynamics is realized. On the other hand, when the function of  $\ln \{-\ln[P(H)]\}$  deviates from a linear dependence of  $H$ , it suggests that the dynamics is not the stochastic one but intermediate or deterministic one.

Applying the formula (17) or (18) to time evolution simulation under a field sweep, we estimate  $H_0$  and  $\beta E_0$  (optimized values). From the values of  $H_0$  and  $\beta E_0$ , we obtain the coercive field  $H_c$  as follows. The relaxation time is given as  $\tau = \tau_0 \exp(\beta \Delta F)$  for the free-energy barrier  $\Delta F$ , and the coercive field is defined as the threshold field at which the relaxation time is 1 s. Thus,  $\beta \Delta F = 25.3$  for  $\tau = 1$  s and  $\tau_0 = 10^{-11}$  s. From the relation

$$\beta F = \beta E_0 \left( 1 - \frac{H_c}{H_0} \right) = 25.3, \quad (19)$$

the coercive field is given as a function of  $H_0$  and  $\beta E_0$ , i.e.,

$$H_c = H_0 \left( 1 - \frac{25.3}{\beta E_0} \right). \quad (20)$$

We investigate an open-boundary system of  $12 \times 12 \times 9$  unit cells ( $10.56 \text{ nm} \times 10.56 \text{ nm} \times 10.971 \text{ nm}$ ) along the  $a$ ,  $b$ , and  $c$  axes, respectively. It has been confirmed that nucleation occurs from a corner at  $T = 0.46T_c$  in similar system sizes [33,59] including this size [32], and the dipole-dipole interaction has negligible effect in this size [39]. First,  $N$  samples with a down-spin state are prepared, and magnetization reversal under a magnetic field sweep is observed. The magnetic field is swept with a constant velocity ( $v$ ) from a low field ( $H_i$ ) to a high field ( $H_f$ ). For each sample, the per-site magnetization,

$$m = \frac{1}{N_{\text{site}}} \sum_{i=1}^{N_{\text{site}}} S_i^z, \quad (21)$$

where  $N_{\text{site}}$  is the number of the atoms in the system, is computed as a function of  $H$ . We determined the reversal field as the field when the value of  $m$  changes from negative to positive. During the field sweeping, the number of the survival (nonrelaxed) samples,  $N_s(H)$ , is counted as a function of  $H$ .  $P(H)$  is estimated as  $P(H) = \frac{N_s(H)}{N}$ . Then,  $\ln \{-\ln[P(H)]\}$  is plotted vs  $H$ . A demonstration will be given in the next section. Equation (18) or (17) is used as a fitting function for this plot, where  $\beta E_0$  and  $H_0$  are fitting parameters for Eq. (18) and  $\beta E_0$ ,  $H_0$ , and  $c$  are those for Eq. (17).

#### IV. ESTIMATION OF COERCIVE FIELD

We study magnetization reversal under a field sweep from  $H = 3.7 \text{ T}$  to  $H = 4.2 \text{ T}$  for  $0.5 \text{ ns}$  ( $v = 1 \times 10^9 \text{ T/s}$ ). We

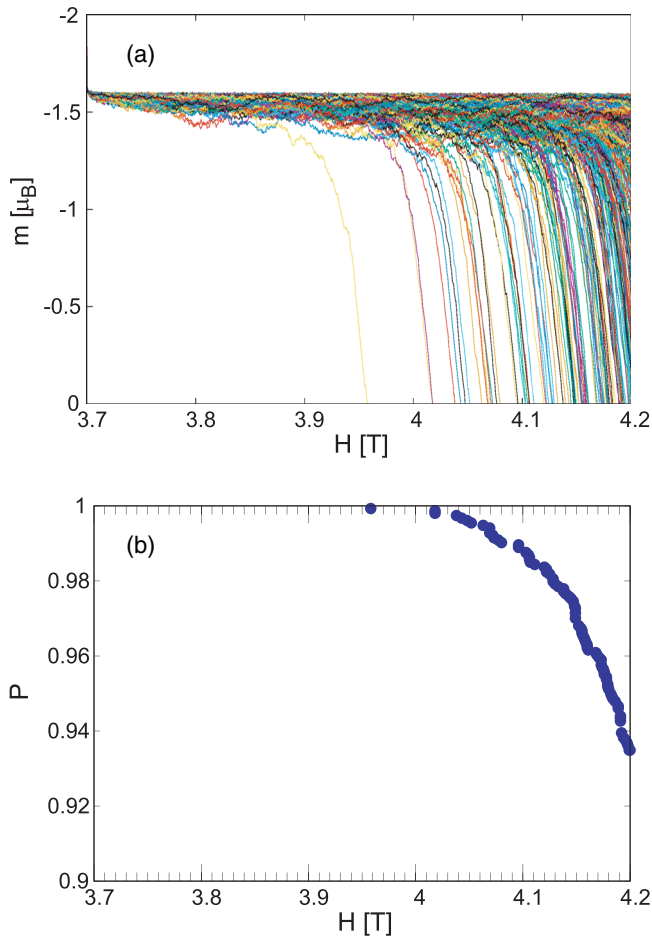


FIG. 3. (a) Magnetization,  $m$ , and (b) survival probability,  $P$ , at  $v = 1 \times 10^9$  T/s under a field sweep from  $H = 3.7$  T to 4.2 T.  $N = 1536$ .  $N_s = 1436$  at  $H = 4.2$  T.

simulate magnetization reversal using  $N = 1536$  samples with different random number sequences for the noise field. Magnetization reversal curves ( $m$ ) and survival probability ( $P(H)$ ) are plotted as a function of the field  $H$  in Fig. 3(a) and Fig. 3(b), respectively. We find that the interval of the reversal field is distributed sparsely and at higher fields the frequency of relaxation increases. In Fig. 4, we find that for  $4.07$  T  $\lesssim H \leq 4.2$  T,  $\ln\{-\ln[P(H)]\}$  shows a rather well defined region with a linear dependence on  $H$ . These observations suggest that the relaxation occurs stochastically for  $4.07$  T  $\lesssim H \leq 4.2$  T. For  $H \gtrsim 4.07$  T, however, we find a deviation from the linear dependence. This region suggests the existence of an initial transient process before a regular relaxation process, which we also encountered in the observation of magnetization relaxation with time dependence for a fixed field in the previous study. This range should be excluded from the coercivity analysis.

Using the function (18), we perform a least-squares fit to the data in the region of  $4.07$  T  $\leq H \leq 4.2$  T, which is shown by the line in Fig. 4. The intercept on the vertical axis  $\ln\{-\ln[P(H)]\}$ , which corresponds to  $\ln[e^{-\beta E_0} \frac{H_0}{v\tau_0\beta E_0}]$ , and the slope of the fitting line, which corresponds to  $\frac{\beta E_0}{H_0}$ , permit calculation of the fitting parameters as  $H_0 = 4.46$  T

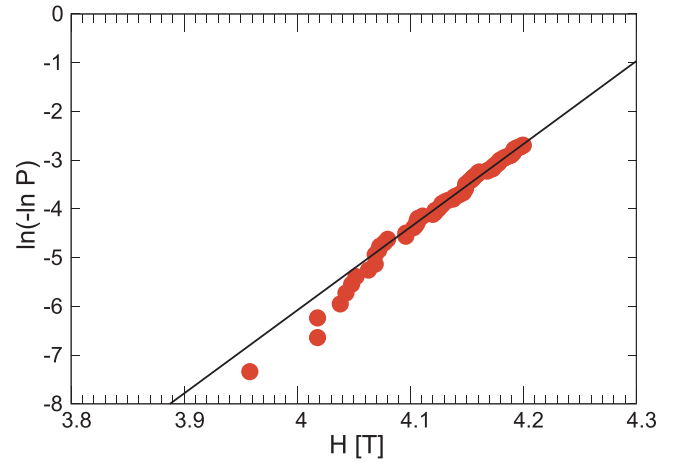


FIG. 4.  $\ln\{-\ln[P(H)]\}$  (red circles) under a field sweep at  $v = 1 \times 10^9$  T/s from  $H = 3.7$  T to 4.2 T. Solid line represents the result of fitting with Eq. (18) (see text for details).

and  $\beta E_0 = 76.0$ . Thus, using the formula (20) with these  $H_0$  and  $\beta E_0$ , the coercive field is obtained as  $H_c = 2.98$  T. We find that this value is very close to the previous estimation of the coercive field ( $H_c \simeq 3.0$ – $3.2$  T) in the same grain, which indicates the capability of the present method to reproduce a compatible result.

If we adopt a different fitting range, e.g.,  $4.02$  T  $\leq H \leq 4.2$  T, the estimated coercive field  $H_c = 3.05$  T is even closer to our anterior result of  $H_c \simeq 3.0$ – $3.2$  T: the fitting values for this case are  $H_0 = 4.44$  T and  $\beta E_0 = 81.1$ . Even if the fitting range is chosen as  $0.3958$  T  $\leq H \leq 4.2$  T, which includes the first relaxation point and the initial transient process (inadequate choice), we find that the estimated coercive field,  $H_c = 3.10$  T, is also close to  $H_c = 2.98$  T. The estimated values for  $H_c$ ,  $H_0$ , and  $\beta E_0$  for different fitting ranges are summarized in Table I. We find that the values of  $H_c$  and  $H_0$  do not change much depending on the fitting range. Because a rather well defined linear region exists, these fittings in different ranges give similar values. The difference in the values gives uncertainty of the present estimation, which is not very small, but the estimated values are in an acceptable range.

Next, we investigate magnetization relaxation under a faster field sweep ( $v = 1.4 \times 10^9$  T/s) in a wider field region (from  $H = 3.8$  T to  $H = 4.5$  T for 0.5 ns) for  $N = 1536$ . In Fig. 5(a) and Fig. 5(b), magnetization reversal curves ( $m$ ) and survival probability [ $P(H)$ ] are presented, respectively, as a function of the field  $H$ . Here, the number of nonrelaxed sam-

TABLE I. Estimated values of  $H_c$ ,  $H_0$ , and  $\beta E_0$  using Eq. (18) in the fitting range between  $H_i$  and  $H_f$  for a field sweep at  $v = 1 \times 10^9$  T/s from  $H = 3.7$  T to 4.2 T. The field values are given in teslas. The values in parentheses are standard errors.

$[H_i, H_f]$	$H_c$	$H_0$	$\beta E_0$
[4.07, 4.2]	2.98(2)	4.461(4)	$7.60(7) \times 10^1$
[4.02, 4.2]	3.05(2)	4.437(4)	$8.11(9) \times 10^1$
[3.958, 4.2]	3.10(2)	4.423(5)	$8.44(10) \times 10^1$

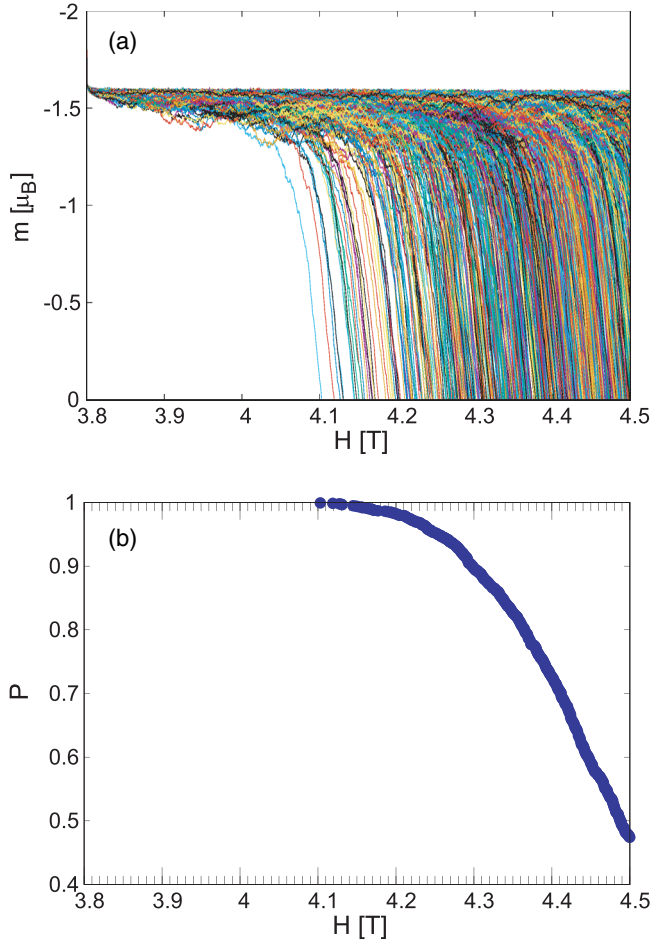


FIG. 5. (a) Magnetization,  $m$ , and (b) survival probability,  $P$ , under a field sweep at  $v = 1.4 \times 10^9$  T/s from  $H = 3.8$  T to 4.5 T.  $N = 1536$ .  $N_s = 728$  at  $H = 4.5$  T.

ples ( $N_s = 728$ ) is smaller than that illustrated in Fig. 3 ( $N_s = 1436$ ), and relaxation data points are packed more densely at the higher field values ( $0.43 \text{ T} \lesssim H$ ).

In Fig. 6,  $\ln\{-\ln[P(H)]\}$  is depicted as a function of  $H$ . We discern three characteristic regions in this plot, i.e., region I: the initial transient region for  $4.1 \text{ T} \lesssim H \lesssim 4.15 \text{ T}$ , in which the data deviate from the dependence shown by the line for Eq. (17); region II: a linear dependence for  $4.15 \text{ T} \lesssim H \lesssim 4.3 \text{ T}$ ; and region III: a bending curve for  $4.3 \text{ T} \lesssim H \lesssim 4.5 \text{ T}$ . Region II suggests a stochastic relaxation region [Fig. 2(a)], and region III indicates an intermediate [Fig. 2(b)] or deterministic region [Fig. 2(c)].

In this case, we use Eq. (17) with three fitting parameters  $H_0$ ,  $\beta E_0$ , and  $c$ . We perform a least-squares fitting to the data in the region of  $4.15 \text{ T} \leq H \leq 4.5 \text{ T}$ . We obtain the coercive field  $H_c = 3.11 \text{ T}$ , and optimized values:  $H_0 = 4.49 \text{ T}$ ,  $\beta E_0 = 82.6$ , and  $c = 17.3$ . If the fitting range is shifted as  $4.12 \text{ T} \leq H \leq 4.5 \text{ T}$ ,  $H_c = 3.19 \text{ T}$  and  $H_0 = 4.47 \text{ T}$  are obtained, and the estimated values of the coercive field  $H_c$  and optimized  $H_0$  hardly change. The relative percentage of the change for  $H_c$  with the values of 3.11 and 3.19 is  $(3.19 - 3.11)/3.11 \times 100\% = 2.57\%$ , and that for  $H_0$  with the values of 4.49 and 4.47 is  $(4.49 - 4.47)/4.49 \times 100\% = 0.445\%$ . Even if the fitting range is changed as  $4.1 \text{ T} \leq H \leq 4.5 \text{ T}$

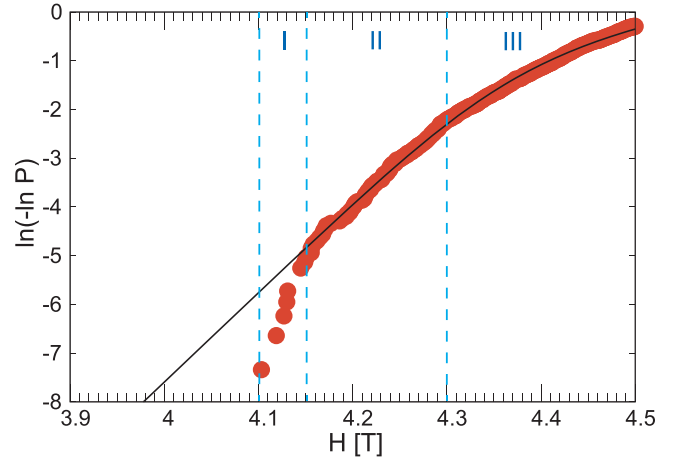


FIG. 6.  $\ln\{-\ln[P(H)]\}$  (red circles) under a field sweep at  $v = 1.4 \times 10^9$  T/s from  $H = 3.8$  T to 4.5 T. Solid curve represents the result of fitting with Eq. (17) (see text for details).

(unphysical choice), which includes the first relaxation point, the estimated values are  $H_c = 3.26 \text{ T}$  and  $H_0 = 4.45 \text{ T}$ , which are close to the values obtained for  $4.15 \text{ T} \leq H \leq 4.5 \text{ T}$ . Estimated values are summarized in Table II. We also find that the values of  $H_c$  and  $H_0$  are not much affected by the choice of the fitting region.

As a reference to the estimation using Eq. (17), we also perform a least-squares fit using Eq. (18) for this data, and compare the results. The fitted line is given in Fig. 7 in the fitting range of  $4.15 \text{ T} \leq H \leq 4.3 \text{ T}$ . We find that the estimated values,  $H_c = 3.09 \text{ T}$ ,  $H_0 = 4.50 \text{ T}$ , and  $\beta E_0 = 80.7$ , are very close to those estimated applying Eq. (17). Estimated values in different fitting ranges are given in Table III. We again find that the estimated  $H_c$  and  $H_0$  are almost the same between the two methods using Eqs. (18) and (17). Compared to  $H_c$  and  $H_0$ ,  $\beta E_0$  is more sensitive to the fitting range.

We estimated  $H_c$ ,  $H_0$ , and  $\beta E_0$  in two different sweepings.  $P(H)$  reduces to 0.935 from  $H = 3.7$  to 4.2 T, while  $P(H)$  reduces to 0.474 from  $H = 3.8$  to 4.5 T. The former is a slow sweeping case, while the latter is a fast sweeping case. Although region III corresponding to the deterministic relaxation appears in the fast sweeping, the values of  $H_c$ ,  $H_0$ , and  $\beta E_0$  in the fast sweeping are still estimated to be close to those in the slow sweeping.

However, in faster sweeping, the region II shrinks (region III dominates) and it becomes difficult to estimate the coercive field. It gives the limitation of applicability of the present method.

TABLE II. Estimated values of  $H_c$ ,  $H_0$ , and  $\beta E_0$  using Eq. (17) in the fitting range between  $H_i$  and  $H_f$  for a field sweep at  $v = 1.4 \times 10^9$  T/s from  $H = 3.8$  T to 4.5 T. The field values are given in teslas. The values in parentheses are standard errors.

$[H_i, H_f]$	$H_c$	$H_0$	$\beta E_0$	$c$
[4.15, 4.5]	3.11(1)	4.486(2)	$8.26(5) \times 10^1$	$1.73(2) \times 10^1$
[4.12, 4.5]	3.19(2)	4.466(3)	$8.83(7) \times 10^1$	$1.92(4) \times 10^1$
[4.10, 4.5]	3.26(2)	4.447(3)	$9.45(10) \times 10^1$	$2.11(5) \times 10^1$

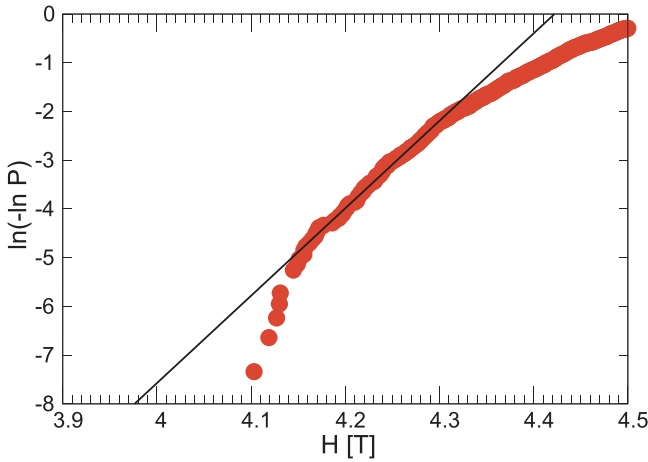


FIG. 7.  $\ln\{-\ln[P(H)]\}$  (red circles) under a field sweep at  $v = 1.4 \times 10^9$  T/s from  $H = 3.8$  T to 4.5 T. Solid line represents the result of fitting with Eq. (18) (see text for details).

From the above analyses, we obtain  $H_c \simeq 3.0\text{--}3.1$  T,  $H_0 \simeq 4.4\text{--}4.5$  T ( $H_c/H_0 \simeq 0.67\text{--}0.69$ ), and  $\beta E_0 \simeq 76\text{--}83$ . For  $T = 0.46T_c = 400$  K in the simulation,  $E_0/k_B \simeq 30\,400\text{--}33\,200$  K. We found that the value of  $H_c$  is very close to that estimated by the previously developed method, i.e.,  $H_c \simeq 3.0\text{--}3.2$  T. In the present method, we need not to obtain the relaxation times for several values of the field. Thus, we conclude that the present method can estimate coercivity approximately with much less effort compared to the previous one. Furthermore, this method can evaluate not only  $H_c$  but also  $H_0$  and  $E_0\beta$ , which is another merit of this method.

In the present work, we used the formula of the potential barrier:  $E_B(H) = E_0(1 - \frac{H}{H_0})^n$  with  $n = 1$  using Eqs. (17) and (18), which produced fitting results with good precision. As was mentioned in the Introduction, the discussion about the proper choice of  $n$  is not settled yet. Here we show that  $n = 1$  is suitable for simulation of nucleation-triggered magnetization reversal in a Nd magnet.

Following the Introduction section, let us recall that coercive field is changed, in addition to physical properties of individual grains, also by conditions of grain boundaries and some other parameters. Quantitative comparison with experimentally estimated coercive fields is out of the scope of the paper, because our objective is to estimate the coercive field of a single grain while experimental systems are assemblies of grains. Here, we just introduce experimental situation of coercive fields of Nd<sub>2</sub>Fe<sub>14</sub>B magnets. References [21,51] reported that  $H_c$ ,  $H_0$ , and  $E_0/k_B$  were estimated for 25–200 °C in two types of hot-deformed Nd-Fe-B magnets: an as-hot-deformed

TABLE III. Estimated values of  $H_c$ ,  $H_0$ , and  $\beta E_0$  using Eq. (18) in the fitting range between  $H_i$  and  $H_f$  for a field sweep at  $v = 1.4 \times 10^9$  T/s from  $H = 3.8$  T to 4.5 T. The field values are given in teslas. The values in parentheses are standard errors.

$[H_i, H_f]$	$H_c$	$H_0$	$\beta E_0$
[4.15, 4.3]	3.09(1)	4.499(2)	$8.07(5) \times 10^1$
[4.12, 4.34]	3.07(2)	4.508(4)	$7.95(9) \times 10^1$
[4.1, 4.4]	2.95(3)	4.548(4)	$7.22(9) \times 10^1$

(HD) magnet and a Nd-Cu eutectic alloy grain-boundary diffused (GBD) magnet. Estimated values at  $25^\circ\text{C} \simeq 0.5T_c$  in experiments [21] are  $H_c = 1.1$  T for HD and  $H_c = 2.2$  T for GBD,  $H_c/H_0 = 0.78$  for HD and  $H_c/H_0 = 0.86$  for GBD, and  $E_0/k_B = 40\,000$  K for HD and  $E_0/k_B = 60\,000$  K for GBD. Although the values of  $H_c$  in experiments are smaller due to the ensemble effects, we consider that our estimation may be a good reference for further development of studies on coercive field. Indeed, the coercive field value depends on sample preparation technique and can reach  $H_c \simeq 3$  T [60].

## V. SUMMARY

We propose a new method for coercive field estimation, which is robust and convenient, because it does not require ample magnetization simulations reaching long observation times characteristic to the experimental studies. Our results can be obtained faster, and moreover, the algorithmic implementation of this new method can benefit considerably from distributed calculations and parallel computing.

Using this method, we estimated the coercive field of a single grain of the Nd magnet. Depending on the field-sweep region, the feature of dynamics varies as stochastic, crossover, and deterministic ones at lower, middle, and higher field regions, respectively. This method works well if the sweep range includes the stochastic relaxation region. When the field sweep is within the stochastic region, Eq. (18) is available, while when it spans over the stochastic region to deterministic region, Eq. (17) is available.

In general, the reversal frequency is low in the stochastic region, which tends to lead to insufficient sampling to  $P(H)$ , and the use of Eq. (17) may be practical for faster relaxation in faster sweeping. In addition to the estimation of coercive field  $H_c$ , this method provides the estimation of zero-field energy barrier  $\beta E_0$  and field for zero-energy barrier  $H_0$ , which are important indices in experimental analyses of coercivity.

When we perform a fitting using Eq. (18) or Eq. (17) to estimate coercivity, the relaxation data in the initial transient process before the regular relaxation in the stochastic region of the field should be excluded. However, exact identification of the border between the initial transient and regular relaxation regions is not necessary, because the values of coercive field and field for zero-energy barrier are not much affected by the fitting range, and it is possible to estimate approximately  $H_c$  and  $H_0$ . The zero-energy barrier  $\beta E_0$  is also well estimated, although it is more sensitive to the fitting range.

We used  $E_B(H) = E_0(1 - \frac{H}{H_0})^n$  assuming  $n = 1$  for the potential barrier in the formulation of Eqs. (17) and (18). Indeed, the estimated  $H_c$  using  $n = 1$  was closer to the previously estimated one than using  $n = 2$ , and the adoption of  $n = 1$  was found to be valid for the estimation of  $H_c$ .

## ACKNOWLEDGMENTS

The authors would like to thank Prof. Okamoto and Dr. Hirotsawa for useful discussions about experimental estimations of coercive field, zero-field energy barrier, and field for zero-energy barrier, and experimental features of the Nd magnet. The present work was supported by the Elements Strategy Initiative Center for Magnetic Materials (ESICMM)

(Grant No. 12016013) funded by the Ministry of Education, Culture, Sports, Science, and Technology (MEXT) of Japan, and was partially supported by Grants-in-Aid for Scientific Research C (No. 18K03444 and No. 20K03809) from MEXT. The numerical calculations were performed on the Numerical Materials Simulator at the National Institute for Materials Science.

### APPENDIX: ESTIMATION OF COERCIVE FIELD USING $n = 2$

In the present study, we adopted  $n = 1$  for Eq. (11). Here, we mention the adoption of  $n = 2$ . In this Appendix, we show the estimation of  $H_c$ ,  $H_0$ , and  $\beta E_0$  using  $n = 2$ .

If  $E_B(H) = E_0(1 - \frac{H}{H_0})^2$  is adopted, the survival probability is

$$P(H) = \exp \left[ -\frac{1}{v\tau_0} \int_{-\infty}^H \frac{1}{e^{\beta E_0(1 - \frac{h}{H_0})^2} + c} dh \right]. \quad (\text{A1})$$

It is difficult to obtain analytical solution for the integral (A1), so we consider a simplified case with  $c = 0$ .

Using the relation

$$\begin{aligned} \int_{-\infty}^H e^{-\beta E_0(1 - \frac{h}{H_0})^2} dh &= \left( \int_{-\infty}^{H_0} dh + \int_{H_0}^H dh \right) e^{-\frac{\beta E_0}{H_0^2} (h - H_0)^2} \\ &= \int_{-\infty}^0 e^{-\frac{\beta E_0}{H_0^2} x^2} dx + \frac{H_0}{\sqrt{\beta E_0}} \int_0^{X_0} e^{-x^2} dx \\ &= \frac{1}{2} \sqrt{\frac{\pi}{\beta E_0}} H_0 [1 + \text{erf}(X_0)], \end{aligned} \quad (\text{A2})$$

where  $X_0 = \frac{\sqrt{\beta E_0}}{H_0} (H - H_0)$ , we have

$$P(H) = \exp \left[ -\frac{1}{2v\tau_0} \sqrt{\frac{\pi}{\beta E_0}} H_0 [1 + \text{erf}(X_0)] \right]. \quad (\text{A3})$$

Then, we obtain

$$\ln\{-\ln[P(H)]\} = \ln \frac{1}{2v\tau_0} \sqrt{\frac{\pi}{\beta E_0}} H_0 [1 + \text{erf}(X_0)]. \quad (\text{A4})$$

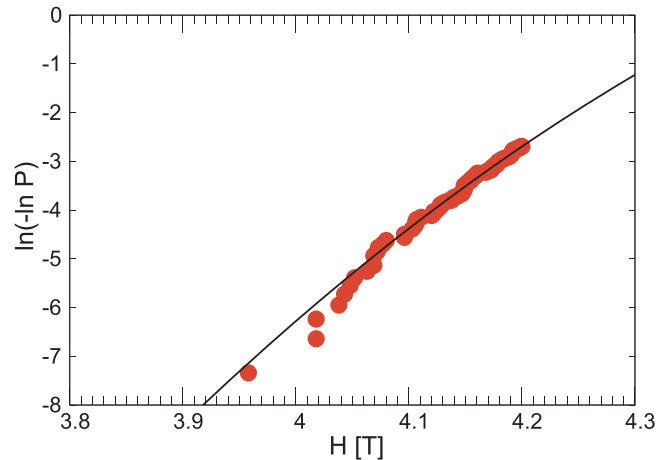


FIG. 8.  $\ln\{-\ln[P(H)]\}$  (red circles) under a field sweep at  $v = 1 \times 10^9$  T/s from  $H = 3.7$  T to 4.2 T. Solid curve represents the result of fitting with Eq. (A4) (see text for details).

TABLE IV. Estimated values of  $H_c$ ,  $H_0$ , and  $\beta E_0$  using Eq. (A4) in the fitting range between  $H_i$  and  $H_f$  for a field sweep at  $v = 1 \times 10^9$  T/s from  $H = 3.7$  T to 4.2 T. The field values are given in teslas. The values in parentheses are standard errors.

$[H_i, H_f]$	$H_c$	$H_0$	$\beta E_0$
[4.07, 4.2]	3.34(2)	4.830(8)	$2.67(5) \times 10^2$
[4.02, 4.2]	3.39(2)	4.790(8)	$2.94(6) \times 10^2$
[3.958, 4.2]	3.40(2)	4.775(8)	$3.05(6) \times 10^2$

Once  $H_0$  and  $\beta E_0$ , i.e., fitting parameters, are obtained,  $H_c$  is estimated in the same manner as the derivation of Eq. (20). From the relation

$$\beta F = \beta E_0 \left(1 - \frac{H_c}{H_0}\right)^2 = 25.3, \quad (\text{A5})$$

the coercive field is given as a function of  $H_0$  and  $\beta E_0$ , i.e.,

$$H_c = H_0 \left(1 - \sqrt{\frac{25.3}{\beta E_0}}\right). \quad (\text{A6})$$

In Fig. 8, we perform a least-squares fit using Eq. (A4) to the data of  $\ln\{-\ln[P(H)]\}$  in the region of  $4.07 \text{ T} \leq H \leq 4.2 \text{ T}$ , studied in Fig. 4. We find that the function Eq. (A4) shows a gently bending curve. The estimated  $H_c$ ,  $H_0$ , and  $\beta E_0$  are 3.34 T, 4.83 T, and 267, respectively. Those in different fitting ranges are summarized in Table IV. In Fig. 9, we also perform a least-squares fit using Eq. (A4) to the data of  $\ln\{-\ln[P(H)]\}$  in the region of  $4.15 \text{ T} \leq H \leq 4.3 \text{ T}$ , investigated in Fig. 6. The estimated  $H_c$ ,  $H_0$ , and  $\beta E_0$  are 3.48 T, 4.81 T, and 329, respectively. Those in different fitting ranges are summarized in Table V. The estimated values of  $H_c$  and  $H_0$  are not much affected by the fitting region, which is the same tendency as the  $n = 1$  case.

We find that the estimated  $H_c$  using Eq. (18) or Eq. (17) is closer to the previously estimated  $H_c$  than that using Eq. (A4), although that using Eq. (A4) slightly overestimates  $H_c$ .

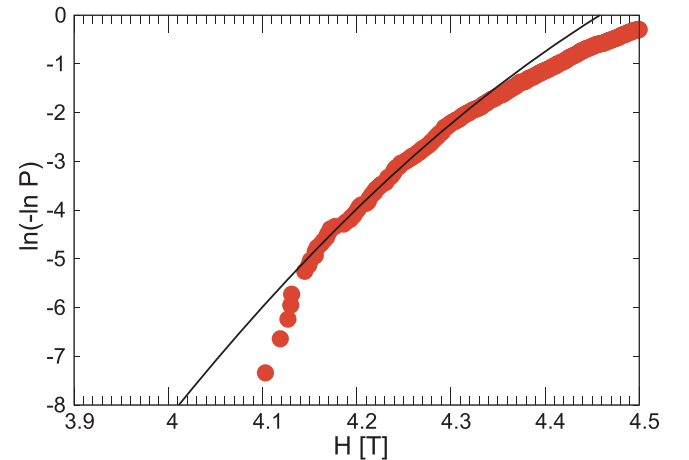


FIG. 9.  $\ln\{-\ln[P(H)]\}$  (red circles) under a field sweep at  $v = 1.4 \times 10^9$  T/s from  $H = 3.8$  T to 4.5 T. Solid curve represents the result of fitting with Eq. (A4) (see text for details).



TABLE V. Estimated values of  $H_c$ ,  $H_0$ , and  $\beta E_0$  using Eq. (A4) in the fitting range between  $H_i$  and  $H_f$  for a field sweep at  $v = 1.4 \times 10^9$  T/s from  $H = 3.8$  T to 4.5 T. The field values are given in teslas. The values in parentheses are standard errors.

$[H_i, H_f]$	$H_c$	$H_0$	$\beta E_0$
[4.15, 4.3]	3.48(1)	4.812(4)	$3.29(4) \times 10^2$
[4.12, 4.34]	3.49(2)	4.809(6)	$3.34(6) \times 10^2$
[4.1, 4.4]	3.44(2)	4.852(7)	$3.00(6) \times 10^2$

Therefore, from the better correspondence of  $H_c$  to the previously estimated  $H_c$ , we conclude that the adoption of  $n = 1$  is more adequate to study the coercive field than that of  $n = 2$ .

As a reference data, the features of the estimated quantities using  $n = 2$  are mentioned:  $H_0 \simeq 4.8$  T and  $H_c/H_0 \simeq 0.69\text{--}0.72$  using  $n = 2$  are a little higher than those using  $n = 1$ , and  $\beta E_0 \simeq 267\text{--}334$  is three or four times larger. This corresponds to  $E_0/k_B \simeq 110\,400\text{--}133\,600$  K.

- [1] M. Sagawa and S. Hirosawa, Magnetic hardening mechanism in sintered R-Fe-B permanent magnets, *J. Mater. Res.* **3**, 45 (1988).
- [2] J. F. Herbst, J. J. Croat, F. E. Pinkerton, and W. B. Yelon, Relationships between crystal structure and magnetic properties in Nd<sub>2</sub>Fe<sub>14</sub>B, *Phys. Rev. B* **29**, 4176 (1984).
- [3] S. Hirosawa, Y. Matsuura, H. Yamamoto, S. Fujimura, M. Sagawa, and H. Yamauchi, Single crystal measurements of anisotropy constants of R<sub>2</sub>Fe<sub>14</sub>B (R=Y, Ce, Pr, Nd, Gd, Tb, Dy and Ho), *Jpn. J. Appl. Phys.* **24**, L803 (1985).
- [4] A. V. Andreev, A. V. Deriagin, N. V. Kudrevatykh, N. V. Mushnikov, and V. A. Reimer, The magnetism of Y<sub>2</sub>Fe<sub>14</sub>B and Nd<sub>2</sub>Fe<sub>14</sub>B and their hydrides, *Zh. Eksp. Teor. Fiz.* **90**, 1042 (1986) [*Sov. Phys. JETP* **63**, 608 (1986)].
- [5] H. Kronmüller, K.-D. Durst, and M. Sagawa, Analysis of the magnetic hardening mechanism in RE-FeB permanent magnets, *J. Magn. Magn. Mater.* **74**, 291 (1988).
- [6] J. F. Herbst, R<sub>2</sub>Fe<sub>14</sub>B materials: Intrinsic properties and technological aspects, *Rev. Mod. Phys.* **63**, 819 (1991).
- [7] S. Hirosawa, Y. Matsuura, H. Yamamoto, S. Fujimura, M. Sagawa, and H. Yamauchi, Magnetization and magnetic anisotropy of R<sub>2</sub>Fe<sub>14</sub>B measured on single crystals, *J. Appl. Phys.* **59**, 873 (1986).
- [8] O. Yamada, Y. Ohtsu, F. Ono, M. Sagawa, and S. Hirosawa, Magnetocrystalline anisotropy in Nd<sub>2</sub>Fe<sub>14</sub>B intermetallic compound, *J. Magn. Magn. Mater.* **70**, 322 (1987).
- [9] N. V. Mushnikov, P. B. Terent'ev, and E. V. Rosenfel'd, Magnetic anisotropy of the Nd<sub>2</sub>Fe<sub>14</sub>B compound and its hydride Nd<sub>2</sub>Fe<sub>14</sub>BH<sub>4</sub>, *Phys. Met. Metallogr.* **103**, 39 (2007).
- [10] K. Hirota, H. Nakamura, T. Minowa, and M. Honshima, Coercivity enhancement by the grain boundary diffusion process to Nd-Fe-B sintered magnets, *IEEE Trans. Magn.* **42**, 2909 (2006).
- [11] R. Ishii, T. Miyoshi, H. Kanekiyo, and S. Hirosawa, High-coercivity nanocomposite permanent magnet based on Nd-Fe-B-Ti-C with Cr addition for high-temperature applications, *J. Magn. Magn. Mater.* **312**, 410 (2007).
- [12] S. Sugimoto, Current status and recent topics of rare-earth permanent magnets, *J. Phys. D* **44**, 064001 (2011).
- [13] K. Lu, X. Bao, G. Chen, X. Mu, X. Zhang, X. Lv, Y. Ding, and X. Gao, Coercivity enhancement of Nd-Fe-B sintered magnet by grain boundary diffusion process using Pr-Tb-Cu-Al alloys, *J. Magn. Magn. Mater.* **477**, 237 (2019).
- [14] R. Friedberg and D. I. Paul, New Theory of Coercive Force of Ferromagnetic Materials, *Phys. Rev. Lett.* **34**, 1234 (1975).
- [15] A. Sakuma, S. Tanigawa, and M. Tokunaga, Micromagnetic studies of inhomogeneous nucleation in hard magnets, *J. Magn. Magn. Mater.* **84**, 52 (1990).
- [16] A. Sakuma, The theory of inhomogeneous nucleation in uniaxial ferromagnets, *J. Magn. Magn. Mater.* **88**, 369 (1990).
- [17] S. Mohakud, S. Andraus, M. Nishino, A. Sakuma, and S. Miyashita, Temperature dependence of the threshold magnetic field for nucleation and domain wall propagation in an inhomogeneous structure with grain boundary, *Phys. Rev. B* **94**, 054430 (2016).
- [18] A. L. Wysocki and V. P. Antropov, Micromagnetic simulations with periodic boundary conditions: Hard-soft nanocomposites, *J. Magn. Magn. Mater.* **428**, 274 (2017).
- [19] I. E. Uysal, M. Nishino, and S. Miyashita, Magnetic field threshold for nucleation and depinning of domain walls in the neodymium permanent magnet Nd<sub>2</sub>Fe<sub>14</sub>B, *Phys. Rev. B* **101**, 094421 (2020).
- [20] Y. Matsuura, J. Hoshijima, and R. Ishii, Relation between Nd<sub>2</sub>Fe<sub>14</sub>B grain alignment and coercive force decrease ratio in NdFeB sintered magnets, *J. Magn. Magn. Mater.* **336**, 88 (2013).
- [21] S. Okamoto, R. Goto, N. Kikuchi, O. Kitakami, T. Akiya, H. Sepehri-Amin, T. Ohkubo, K. Hono, K. Hioki, and A. Hattori, Temperature-dependent magnetization reversal process and coercivity mechanism in Nd-Fe-B hot-deformed magnets, *J. Appl. Phys.* **118**, 223903 (2015).
- [22] T. Pramanik, A. Roy, R. Dey, A. Rai, S. Guchhait, H. C. Movva, C.-C. Hsieh, and S. K. Banerjee, Angular dependence of magnetization reversal in epitaxial chromium telluride thin films with perpendicular magnetic anisotropy, *J. Magn. Magn. Mater.* **437**, 72 (2017).
- [23] D. Givord, A. Lienard, P. Tenaud, and T. Viadieu, Magnetic viscosity in Nd-Fe-B sintered magnets, *J. Magn. Magn. Mater.* **67**, L281 (1987).
- [24] D. Givord, P. Tenaud, and T. Viadieu, Coercivity mechanisms in ferrites and rare earth transition metal sintered magnets (SmCo<sub>5</sub>, Nd-Fe-B), *IEEE Trans. Magn.* **24**, 1921 (1988).
- [25] D. Givord, P. Tenaud, and T. Viadieu, Angular dependence of coercivity in sintered magnets, *J. Magn. Magn. Mater.* **72**, 247 (1988).
- [26] Y. Toga, M. Matsumoto, S. Miyashita, H. Akai, S. Doi, T. Miyake, and A. Sakuma, Monte Carlo analysis for finite-temperature magnetism of Nd<sub>2</sub>Fe<sub>14</sub>B permanent magnet, *Phys. Rev. B* **94**, 174433 (2016).
- [27] M. Nishino, Y. Toga, S. Miyashita, H. Akai, A. Sakuma, and S. Hirosawa, Atomistic-model study of temperature-dependent domain walls in the neodymium permanent magnet Nd<sub>2</sub>Fe<sub>14</sub>B, *Phys. Rev. B* **95**, 094429 (2017).

- [28] T. Hinokihara, M. Nishino, Y. Toga, and S. Miyashita, Exploration of the effects of dipole-dipole interactions in  $\text{Nd}_2\text{Fe}_{14}\text{B}$  thin films based on a stochastic cutoff method with a novel efficient algorithm, *Phys. Rev. B* **97**, 104427 (2018).
- [29] S. Miyashita, M. Nishino, Y. Toga, T. Hinokihara, T. Miyake, S. Hirose, and A. Sakuma, Perspectives of stochastic micromagnetism of  $\text{Nd}_2\text{Fe}_{14}\text{B}$  and computation of thermally activated reversal process, *Scr. Mater.* **154**, 259 (2018).
- [30] Y. Toga, M. Nishino, S. Miyashita, T. Miyake, and A. Sakuma, Anisotropy of exchange stiffness based on atomic-scale magnetic properties in the rare-earth permanent magnet  $\text{Nd}_2\text{Fe}_{14}\text{B}$ , *Phys. Rev. B* **98**, 054418 (2018).
- [31] M. Nishino and S. Miyashita, Nontrivial temperature dependence of ferromagnetic resonance frequency for spin reorientation transitions, *Phys. Rev. B* **100**, 020403(R) (2019).
- [32] M. Nishino, I. E. Uysal, T. Hinokihara, and S. Miyashita, Dynamical aspects of magnetization reversal in the neodymium permanent magnet by a stochastic Landau-Lifshitz-Gilbert simulation at finite temperature: Real-time dynamics and quantitative estimation of coercive force, *Phys. Rev. B* **102**, 020413(R) (2020).
- [33] Y. Toga, S. Miyashita, A. Sakuma, and T. Miyake, Role of atomic-scale thermal fluctuations in the coercivity, *npj Comput. Mater.* **6**, 67 (2020).
- [34] S. Westmoreland, R. Evans, G. Hrkac, T. Schrefl, G. Zimanyi, M. Winklhofer, N. Sakuma, M. Yano, A. Kato, T. Shoji, A. Manabe, M. Ito, and R. Chantrell, Multiscale model approaches to the design of advanced permanent magnets, *Scr. Mater.* **148**, 56 (2018).
- [35] S. C. Westmoreland, C. Skelland, T. Shoji, M. Yano, A. Kato, M. Ito, G. Hrkac, T. Schrefl, R. F. L. Evans, and R. W. Chantrell, Atomistic simulations of  $\alpha\text{-Fe}/\text{Nd}_2\text{Fe}_{14}\text{B}$  magnetic core/shell nanocomposites with enhanced energy product for high temperature permanent magnet applications, *J. Appl. Phys.* **127**, 133901 (2020).
- [36] Q. Gong, M. Yi, R. F. L. Evans, B.-X. Xu, and O. Gutfleisch, Calculating temperature-dependent properties of  $\text{Nd}_2\text{Fe}_{14}\text{B}$  permanent magnets by atomistic spin model simulations, *Phys. Rev. B* **99**, 214409 (2019).
- [37] Q. Gong, M. Yi, and B.-X. Xu, Multiscale simulations toward calculating coercivity of Nd-Fe-B permanent magnets at high temperatures, *Phys. Rev. Mater.* **3**, 084406 (2019).
- [38] Q. Gong, M. Yi, R. F. L. Evans, O. Gutfleisch, and B.-X. Xu, Anisotropic exchange in Nd-Fe-B permanent magnets, *Mater. Res. Lett.* **8**, 89 (2020).
- [39] S. Miyashita, M. Nishino, Y. Toga, T. Hinokihara, I. E. Uysal, T. Miyake, H. Akai, S. Hirose, and A. Sakuma, Atomistic theory of thermally activated magnetization processes in  $\text{Nd}_2\text{Fe}_{14}\text{B}$  permanent magnet, *Sci. Technol. Adv. Mater.* **22**, 658 (2021).
- [40] M. Nishino, I. E. Uysal, and S. Miyashita, Effect of the surface magnetic anisotropy of neodymium atoms on the coercivity in neodymium permanent magnets, *Phys. Rev. B* **103**, 014418 (2021).
- [41] M. Nishino, H. Hayasaka, and S. Miyashita, Microscopic origin of coercivity enhancement by dysprosium substitution into neodymium permanent magnets, *Phys. Rev. B* **106**, 054422 (2022).
- [42] H. Kronmüller and M. Fähnle, *Micromagnetism and the Microstructure of Ferromagnetic Solids*, Cambridge Studies in Magnetism (Cambridge University Press, Cambridge, UK, 2003).
- [43] J. L. García-Palacios and F. J. Lázaro, Langevin-dynamics study of the dynamical properties of small magnetic particles, *Phys. Rev. B* **58**, 14937 (1998).
- [44] M. Nishino and S. Miyashita, Realization of the thermal equilibrium in inhomogeneous magnetic systems by the Landau-Lifshitz-Gilbert equation with stochastic noise, and its dynamical aspects, *Phys. Rev. B* **91**, 134411 (2015).
- [45] R. Dittrich, T. Schrefl, D. Suess, W. Scholz, H. Forster, and J. Fidler, A path method for finding energy barriers and minimum energy paths in complex micromagnetic systems, *J. Magn. Mater.* **250**, 12 (2002).
- [46] W. E, W. Ren, and E. Vanden-Eijnden, Simplified and improved string method for computing the minimum energy paths in barrier-crossing events, *J. Chem. Phys.* **126**, 164103 (2007).
- [47] P. Asselin, R. F. L. Evans, J. Barker, R. W. Chantrell, R. Yanes, O. Chubykalo-Fesenko, D. Hinzke, and U. Nowak, Constrained Monte Carlo method and calculation of the temperature dependence of magnetic anisotropy, *Phys. Rev. B* **82**, 054415 (2010).
- [48] F. Wang and D. P. Landau, Efficient, Multiple-Range Random Walk Algorithm to Calculate the Density of States, *Phys. Rev. Lett.* **86**, 2050 (2001).
- [49] M. Yamada, H. Kato, H. Yamamoto, and Y. Nakagawa, Crystal-field analysis of the magnetization process in a series of  $\text{Nd}_2\text{Fe}_{14}\text{B}$ -type compounds, *Phys. Rev. B* **38**, 620 (1988).
- [50] W. Wernsdorfer, E. B. Orozco, K. Hasselbach, A. Benoit, B. Barbara, N. Demoncy, A. Loiseau, H. Pascard, and D. Mailly, Experimental Evidence of the Néel-Brown Model of Magnetization Reversal, *Phys. Rev. Lett.* **78**, 1791 (1997).
- [51] S. Okamoto, Experimental approaches for micromagnetic coercivity analysis of advanced permanent magnet materials, *Sci. Technol. Adv. Mater.* **22**, 124 (2021).
- [52] R. H. Victora, Predicted Time Dependence of the Switching Field for Magnetic Materials, *Phys. Rev. Lett.* **63**, 457 (1989).
- [53] P. Gaunt, Magnetic viscosity and thermal activation energy, *J. Appl. Phys.* **59**, 4129 (1986).
- [54] T. Pokhil and E. Nikolaev, Domain wall motion in Re-Tm films with different thickness, *IEEE Trans. Magn.* **29**, 2536 (1993).
- [55] K.-J. Kim, J. Ryu, G.-H. Gim, J.-C. Lee, K.-H. Shin, H.-W. Lee, and S.-B. Choe, Electric Current Effect on the Energy Barrier of Magnetic Domain Wall Depinning: Origin of the Quadratic Contribution, *Phys. Rev. Lett.* **107**, 217205 (2011).
- [56] M. Sharrock and J. McKinney, Kinetic effects in coercivity measurements, *IEEE Trans. Magn.* **17**, 3020 (1981).
- [57] M. P. Sharrock, Time dependence of switching fields in magnetic recording media (invited), *J. Appl. Phys.* **76**, 6413 (1994).
- [58] J. de Vries, T. Bolhuis, and L. Abelmann, Temperature dependence of the energy barrier and switching field of sub-micron magnetic islands with perpendicular anisotropy, *New J. Phys.* **19**, 093019 (2017).
- [59] S. Hirose, M. Nishino, and S. Miyashita, Perspectives for high-performance permanent magnets: Applications, coercivity, and new materials, *Adv. Nat. Sci.: Nanosci. Nanotechnol.* **8**, 013002 (2017).
- [60] T.-H. Kim, T. Sasaki, T. Ohkubo, Y. Takada, A. Kato, Y. Kaneko, and K. Hono, Microstructure and coercivity of grain boundary diffusion processed Dy-free and Dy-containing Nd-Fe-B sintered magnets, *Acta Mater.* **172**, 139 (2019).